A&A 618, A5 (2018)
https://doi.org/10.1051/0004-6361/201732156

Astronomy & Astrophysics

Radial velocity survey of spatially resolved young, low-mass binaries⋆

Stephen Durkan[1,2], Markus Janson[2], Simona Ciceri[2], Wolfgang Brandner[3], Joshua Schlieder[4], Thomas Henning[3], Mickaël Bonnefoy[5], Juliet Kankare[1], and Christopher A. Watson[1]

[1] Astrophysics Research Center, Queens University Belfast, Belfast, UK
e-mail: sdurkan01@qub.ac.uk
[2] Department of Astronomy, Stockholm University, Stockholm, Sweden
e-mail: markus.janson@astro.su.se, simona.ciceri@astro.su.se
[3] Max Planck Institute for Astronomy, Heidelberg, Germany
[4] NASA Exoplanet Science Institute, Caltech, Pasadena, CA, USA
[5] Université Grenoble Alpes, IPAG, Grenoble, France

Received 23 October 2017 / Accepted 8 June 2018

ABSTRACT

The identification and characterisation of low-mass binaries is of importance for a range of astrophysical investigations. Low-mass binaries in young (∼10−100 Myr) moving groups (YMGs) in the solar neighborhood are of particular significance as they provide unique opportunities to calibrate stellar models and evaluate the ages and coevality of the groups themselves. Low-mass M-dwarfs have pre-main sequence life times on the order of ∼100 Myr and therefore are continually evolving along a mass-luminosity track throughout the YMG phase, providing ideal laboratories for precise isochronal dating, if a model-independent dynamical mass can be measured. AstraLux lucky imaging multiplicity surveys have recently identified hundreds of new YMG low-mass binaries, where a subsample of M-dwarf multiples have estimated orbital periods less than 50 yr. We have conducted a radial velocity survey of a sample of 29 such targets to complement the astrometric data. This will allow enhanced orbital determinations and precise dynamical masses to be derived in a shorter timeframe than possible with astrometric monitoring alone, and allow for a more reliable isochronal analysis. Here we present radial velocity measurements derived for our sample over several epochs. We report the detection of the three-component spectroscopic multiple 2MASS J05301858-5358483, for which the C component is a new discovery, and forms a tight pair with the B component. Originally identified as a YMG member, we find that this system is a likely old field interloper, whose high chromospheric activity level is caused by tidal spin-up of the tight BC pair. Two other triple systems with a tight pair exist in the sample, 2MASS J04244260-0647313 (previously known) and 2MASS J20163382-0711456, but for the rest of the targets we find that additional tidally synchronized companions are highly unlikely, providing further evidence that their high chromospheric activity levels are generally signatures of youth.

Key words. binaries: spectroscopic – binaries: visual – stars: pre-main sequence

1. Introduction

Low-mass stars in multiple systems are increasingly playing an important role in stellar astrophysics. Statistically constraining their multiplicity characteristics and population properties provides clues on their formation and evolutionary pathways (e.g., Burgasser et al. 2007; Bate 2012; Duchêne & Kraus 2013), potentially connecting higher-mass stars to brown dwarfs (e.g., Luhman et al. 2007; Chabrier et al. 2014). The identification and characterisation of low-mass multiples is also highly relevant to several fields of exoplanet study. For example, direct imaging surveys typically exclude visual binaries (e.g., Lafrenière et al 2007; Janson et al. 2011; Vigan et al. 2012, 2017; Rameau et al. 2013) due to the intricacies of planet detection within the combined point-spread function (PSF) patterns of multiple stars, alongside the formation and long-term stability barriers faced by any possible planet orbiting such systems. Recently however, efforts have also been made to probe the population of wide separation circumbinary planets through dedicated imaging studies of stellar multiples (e.g., Thalmann et al. 2014; Bonavita et al. 2016). Binary identification aids target selection for such studies.

Also of fundamental importance to any imaging study is a good estimate of target age. This is critical for estimating the mass or initial entropy of planets and brown dwarfs using mass-luminosity evolutionary models. Such objects are maximally hot, and therefore luminous, directly after formation and gradually cool — becoming less luminous as the planet ages (Baraffe et al. 2003; Burrows et al. 2003; Fortney et al. 2008). Imaging surveys therefore typically target stars in young moving groups (YMGs) (e.g., Biller et al. 2013; Brandt et al. 2014; Durkan et al. 2016), young (∼10−100 Myr) co-moving associations of stars in the solar neighborhood originating from a common birth cluster (e.g., Zuckerman & Song 2004; Torres et al. 2008). YMGs also provide age estimates of stars that are potentially much more reliable than any accessible technique for individual stars, translating to a more reliable and precise mass estimate of any imaged companion.

⋆ Table 2 is only available in electronic form at the CDS via anonymous ftp to cdsarc.u-strasbg.fr (130.79.128.5) or via http://cdsarc.u-strasbg.fr/viz-bin/qcat?J/A+A/618/A5

However, uncertainties remain in the ages of YMGs. For instance, the age estimates in the AB Dor (e.g., Torres et al. 2008; Baraffe et al. 2013; Bell et al. 2015) and USco (de Zeeuw et al. 1999; Pecaut et al. 2012; Song et al. 2012) associations vary by more than a factor of two between the lowest and highest reasonable estimates in the literature. These age uncertainties, although relatively small compared to field star ages, dominate the mass uncertainty of an imaged sub-stellar companion and can lead to disparity in the mass estimates of analogous studies (e.g., J010335; Delorme et al. 2013; Janson et al. 2017), potentially furthering ambiguity to its interpretation as a planet or brown dwarf. A better understanding of YMG ages is essential for more robust constraints to be placed on companion masses.

In this regard, YMG M-dwarf multiples can be very useful. As M-dwarfs have considerably long pre-main sequence lifetimes (~100 Myr e.g., Baraffe et al. 1998), they are continually evolving along a mass-luminosity track throughout the YMG phase, providing ideal laboratories for precise isochronal dating. Such dating analysis can be conducted using spectral properties alone; bolometric luminosity and effective temperature (e.g., Janson et al. 2007), however, the large degree of uncertainty in the ultra-cool M-dwarf temperature scale introduces a source of systematic error into the analysis. Relating a model independent mass, such as dynamical masses derived from orbitally monitoring M-dwarf multiples, to luminosity allows for a much more robust isochronal analysis. This has been demonstrated for a few YMG binaries (e.g., Bonnefoy et al. 2009; Köhler et al. 2013; Montet et al. 2015) however, a broader comprehensive study is of fundamental importance to cover a wider sample of YMGs and to assess dating robustness and coevality within individual YMGs. Model independent M-dwarf masses can also be derived through high precision photometric and spectroscopic observations of double-lined, eclipsing binaries (e.g., Zhou et al. 2014, 2015). However, such systems are rare and typically much older than any YMG and the ~100 Myr pre-main sequence lifetime.

These arguments for low-mass multiplicity studies and binary characterization have motivated our AstraLux Large M-dwarf Multiplicity surveys, systematic lucky imaging studies of >1000 X-ray active young M-dwarfs, many of which are also high probability YMG members (e.g., Bergfors et al. 2010; Janson et al. 2012, 2014a, 2017). As one would expect roughly 30% of these were identified as multiple systems, significantly increasing the number of close YMG M-dwarf binaries. Whilst the ultimate goal of the AstraLux surveys is to derive individual dynamical masses and isochronally date M-dwarf multiples, for improved age constraints on the full YMG population, it is not feasible for the majority of the sample over the current survey lifetime due to the relatively long orbital timescales. However, mass determinations are possible for several systems due to particularly short orbital periods and/or wealth of additional astrometric data in the literature (e.g., Calissendorff et al. 2017).

However, astrometric monitoring alone is often not enough to derive precise dynamical masses and enable a robust isochronal analysis, a complementary radial velocity (RV) analysis is equally important for a range of purposes. Whilst relative astrometry provides the means to constrain orbital parameters, it is limited to providing the total system mass. An RV analysis provides information about the mass ratio of the system, allowing individual component masses to be derived when coupled with the astrometric information. RV data also provides a third dimension of information, outside the plane of the sky, providing much stronger constraints on mutual orbital parameters (e.g., period, eccentricity, argument of periapsis etc.) in a shorter timeframe than would be possible with either method in isolation (Tuomi et al. 2009). An additional importance to the RV observations is the ability to efficiently detect further close companions in the system that are unresolved in the images. Identifying such companions is of critical importance for isochronal analysis as any unresolved pair treated as a single star will lead to an incorrect age estimate or model calibration.

Motivated by this reasoning we have conducted an RV monitoring survey of a sample of 29 high-utility M-dwarf binaries to complement our astrometric observations. As precise mass determinations combining astrometric and RV measurements will only become possible over a several year timescale (in order to sufficiently sample and nearly close orbits) for the majority of the targets, we do not present any individual mass estimates or isochronal analysis here. Instead, we present a spectral analysis of two unique systems that are suspected to host unresolved tidally synchonized companions, and list radial velocities for the sample over several epochs. These measurements will be vital for determining masses over the coming years and achieving the long-term goals of the AstraLux surveys. We also evaluate the likelihood of the presence of additional synchronized companions in the sample.

2. Target sample

In our previous AstraLux M-dwarf multiplicity studies, targets were selected from multiple catalogs of late type stars on the basis of youth; indicated by high-probability YMG membership (e.g., Malo et al. 2013, 2014; Kraus et al. 2014) and X-ray emission (Lépine & Gaidos 2011). These studies have detected >300 confirmed M-dwarf binaries, the majority of which were previously undiscovered. Janson et al. (2014b) identified a subsample of these binaries that exhibit strong indications of youth and estimated orbital periods less than 50 yr. Orbits for these high-utility binaries could be closed on the scale of years to several decades, allowing full orbital parameters and dynamical masses to be constrained within reasonable timeframes.

The target sample in this study is primarily compiled from the Janson et al. (2014b) sub-sample. We selected 21 targets with orbital periods less than 40 yr for complementary RV monitoring. This will allow for full orbital constraints and a robust isochronal analysis to be conducted on a much shorter timescale than would be possible with astrometric monitoring alone. We also selected three youthful systems targeted in Janson et al. (2012) that appeared as single stars in the AstraLux images; J042442, J084756 and J232057. However, these targets have either been previously resolved or are spectroscopic binaries, indicating short component separations and therefore rapid orbital periods. As our unresolved images reveal limited astrometric information, radial velocity monitoring of these targets is the most viable method for producing orbital determinations. From the literature we selected an additional five resolved low-mass binary systems that have strong indications of youth and short orbital periods for which additional RV measurements would significantly enhance orbital determinations; J052844 (Janson et al. 2007), J101726 (Bonnefoy et al. 2009), J120727 (Bonavita et al. 2016), J122021 (Köhler 2001) and J155734 (Lafrenière et al. 2014). Due to the scientific aims of the project, the targets were chosen entirely on individual merit in terms of orbital properties and youth, with no particular considerations regarding sample uniformity in other respects. Our sample is listed in Table 1 along with target spectral type, estimated binary orbital period and YMG/association membership. We note that several systems in our sample have previously been identified as members of the Argus association. However, Bell et al. (2015) suggest that

Table 1. Target sample properties.

2MASS ID	SpT	Period estimate (yr)	YMG/Association	YMG/Association Reference	YMG/Association Age (Myr)
J01112542 + 1526214	M5.0+M6.0	12	β Pic	M14	24 ± 3
J02451431 – 4344102	M4.0+M4.5	13	....		
J02490228 – 1029220	M1.5+M3.5+M3.5	30	β Pic?	B16	24 ± 3
J03323578 + 2843554	M4.0+M4.5+M5.5	8	β Pic	M14, J14	24 ± 3
J04244260 – 0647313	M4.0[1]	<0.2[7]	Argus	M13	40 ± 10[a]
J04373746 – 0229282	M0.0+M3.0	29[8]	β Pic	M13	24 ± 3
J04595855 – 0333123	M4.0+M5.5	9	Argus?	M13, J14	40 ± 10
J05284446 – 6526463	M5.0+M5.5[2]	1.6[2]	AB Dor	LS06	149^{+51}_{-19}
J05301858 – 5358483	M3.0+M4.0+M6.0	25	AB Dor**	M14	149^{+51}_{-19}
J05320450 – 0305291	M2.0+M3.5	23	β Pic?	M13, J14	24 ± 3
J06112997 – 7213388	M4.0+M5.0	8	Carina	M14	45^{+11}_{-7}
J06134539 – 2352077	M3.5+M5.0	13	Argus	M14, J14	40 ± 10
J06161032 – 1320422	M3.5+M5.0	37	β Pic?	M13, J14	24 ± 3
J07285137 – 3014490	M1.5+M3.5	33	AB Dor	M13	$149^{+51}_{-19} \pm$
J08475676 – 7854532	M3.0[3]	....*	η Cha	LM13	11 ± 3[b]
J09075823 + 2154111	M2.0+M3.5	12	....		
J09164398 – 2447428	M0.5+M2.5	10	....		
J10140807 – 7636327	M4.0+M5.5	17	Carina	M14	45^{+11}_{-7}
J10172689 – 5354265	M6.0+M6.0[4]	5.15[4]	β Pic	M13	24 ± 3
J11315526 – 3436272	M2.5+M9.0	5.94[9]	TW Hya	M14	10 ± 3
J12072738 – 3247002	M1.0[5]	4.2[10,11]	TW Hya	M14	10 ± 3
J12202177 – 7407393	M1.0[3]	....*	ϵ Cha	LM13	$\sim$6
J13493313 – 6818291	M2.0+M4.0+M3.5	25	Argus	M13	40 ± 10[a]
J15573430 – 2321123	M1.0[6]	27[12]	Upper Scorpius	R15	11 ± 2[c]
J20163382 – 0711456	M0.0+M2.0	18	Argus**	M14, J14	40 ± 10[a]
J20531465 – 0221218	M3.0+M4.0	13	Argus?	M13	40 ± 10[a]
J23172807 + 1936469	M3.0+M4.5	33	β Pic?	M13, J14	24 ± 3
J23205766 – 0147373	M4.0[1]	....*	Argus	M14	40 ± 10[a]
J23495365 + 2427493	M3.5+M4.5	38	β Pic/Columba?	M13, J14	24 ± 3 / 42^{+6}_{-4}

Notes. Individual spectral types derived by Janson et al. (2012) following the methods of Daemgen et al. (2007), unless otherwise noted. Estimated orbital period based on system mass and approximate semimajor axis taken from Janson et al. (2014b) unless otherwise noted. "?" in column 4 denotes ambiguity in association membership. YMG/Association ages are taken from Bell et al. (2015) unless otherwise noted. (*)Sources are partially resolved or previously resolved at small separations indicating rapid orbital periods (Köhler 2001; Köhler & Petr-Gotzens 2002; Daemgen et al. 2007). (**)J053018 and J201633 YMG membership is highly unlikely following our analysis detailed in Sects. 4.1 and 4.2 respectively. (1)Integrated spectral type (Int SpT); Alonso-Floriano et al. (2015), (2)Janson et al. (2007), (3)Int SpT; Riaz et al. (2006), (4)Bonnefoy et al. (2009), (5)Int SpT; Chauvin et al. (2010), (6)Int SpT; Carpenter et al. (2006), (7)Shkolnik et al. (2010), (8)Montet et al. (2015), (9)Konopacky et al. (2007), (10)Bailey et al. (2012), (11)Bonavita et al. (2016), (12)Lafrenière et al. (2014), (a)Malo et al. (2013), (b)Torres et al. (2008), (c)Pecaut et al. (2012).

References. – B16; Bergfors et al. (2016), J14; Janson et al. (2014b), LM13; López Martí et al. (2013), LS06; López-Santiago et al. (2006), M13; Malo et al. (2013), M14; Malo et al. (2014), R15; Rizzuto et al. (2015), W94; Walter et al. (1994).

Argus is largely contaminated by interlopers and may not represent a single, coeval population. Therefore, it remains unclear if these targets can be associated to any YMG.

3. Observations and data reduction

All of our RV monitoring was conducted using the Fiberfed Extended Range Optical Spectrograph (FEROS; Kaufer et al. 1999) mounted at the ESO-MPG 2.2 m telescope at La Silla Observatory. The observations used in this survey were taken in service mode under programs 093.A-9006(A) and 094.A-9002(A) between September 2014 and October 2015. A maximum of five spectra were taken per target as an optimal trade-off between initial number of RV data points and required observational time. We also choose to include several archival FEROS observations to bolster the number of spectra for targets in which the ideal sample of five was not obtained, for future orbital analysis. RV measurements for these archival spectra have not been previously published and are included in Table 2 with MJD prior to 56912. A further five spectra of J07285137−3014490 were included (taken from archival and ongoing RV monitoring campaigns) in order to significantly increase the number of available RV measurements, enabling a dedicated study of the system (Rodet et al. 2018). FEROS is an echelle spectrograph covering the wavelength range 3500−9200 Angstrom across 39 orders with $R \approx 48\,000$. Observations were carried out in "object+calibration configuration" in which one of the two FEROS optical fibres is centered on the star whilst the other simultaneously observes a ThAr+Ne lamp to monitor spectrograph stability. Afternoon calibrations such as bias frames and flat-fields were also taken for data reduction.

All standard spectroscopic data reduction procedures such as flat-fielding, pixel correction, order extraction and ThAr+Ne lamp wavelength calibration were carried out using the

ESO-MIDAS based FEROS Data Reduction System (DRS). The DRS also carries out a re-binning and order merging to produce an optimally reduced continuous spectrum. Müller et al. (2013) note that the automatic barycentric correction the DRS applies is inaccurate. Therefore we reversed the DRS correction and applied an improved correction based on the algorithm of Stumpff (1980).

In order to derive radial velocity measurements for the sample we cross correlated our observed spectra with synthetic template spectra. Our synthetic spectra were generated from the spectral libraries of Husser et al. (2013). This library is particularly well suited for our purposes as it has been compiled using the ACES equation of state, which accounts for the formation of molecules at the low temperatures of M-dwarf atmospheres. For each target we used a single synthetic template for cross-correlation. The template was generated using surface gravity, temperature and metalicity input parameters. We adopted a solar metalicity for each target as our sample resides in the solar neighborhood. We adopted temperature and surface gravity values from Baraffe et al. (1998) evolutionary models based on estimated target age and mass. These masses are first order approximations, derived from primary component spectral type for resolved stars, and integrated spectral type for unresolved stars using the spectral type-mass relations of Kraus & Hillenbrand (2007). These spectral types are estimated via AstraLux photometry Janson et al. (2012) following the methods of Daemgen et al. (2007), unless otherwise noted in Table 1.

We computed cross-correlation functions for each of the spectra over multiple wavelength ranges. These ranges correspond to the wavelengths of individual echelle orders that are free from telluric and strong stellar emission lines. ~30 orders are suitable for cross correlation for each target, although this value decreases for later spectral types due to lower signal to noise data at shorter wavelengths. The edges of each order range were also clipped to avoid edge of chip effects and any inaccuracy in the DRS order merging. The RV was measured across each range by fitting a Gaussian to the CCF, or multiple Gaussians for multiple component spectroscopic binaries. We then derived a final RV measurement for each spectrum by taking a mean of these individual RV measurements (weighted by the goodness of the Gaussian fit to each CCF) and calculating the uncertainty by computing the standard error.

4. Results and discussion

The results of our RV monitoring survey for our sample of 29 M-dwarf multiples are presented in Table 2. On average, we derive individual RVs to a precision of ~0.2 km s^{-1}, obtaining ~3−4 epochs of measurements per target. An example RV plot is shown in Fig. 1. RV's for the targets J024514, J090758 and J234953 are reported here for the first time, whilst several other targets have RV's reported to sub km s^{-1} precision for the first time. There are two three-component spectroscopic multiples present in this sample, one of which is a new discovery, and which is discussed in the Sect. 4.1. In Sect. 4.2 we also present the new discovery of a suspected single-lined triple system. Further individual targets are discussed in Appendix A.

4.1. High-order multiplicity of 2MASS J05301858−5358483

The system 2MASS J05301858−5358483, hereafter abbreviated as J053018, was previously known to be a M3.0+M4.0+M6.0 resolved triple system. In each of our RV epochs we recover a triple-peaked CCF and therefore identify J053018 as a three-component spectroscopic multiple. An example triple-peaked CCF is shown in Fig. 2. Janson et al. (2012, 2014b) derive a separation of ~0.2″ for the tight M3.0+M4.0 pair, and a separation of ~4″ for the wide M6.0 companion. As the M6.0 companion falls outside the 2.0″ FEROS fibre aperture, the third spectroscopic component is most likely due to an additional unresolved tight companion, making J053018 a quadruple system. As mentioned in Sect. 1, identifying any unresolved components in a multiple system is of critical importance for an accurate isochronal analysis. The RV data for J053018 is plotted in Fig. 3. We identify which spectroscopic component is responsible for each individual RV measurement by tracing CCF peak strength across each epoch. We relate the strongest peak in each epoch to the "A" component, occurring at ~30 km s^{-1} in Fig. 2. The 2nd strongest CCF peak we relate to the "B" component and the lowest strength peak to "C" component, occurring at ~0 km s^{-1} and ~70 km s^{-1} respectively in Fig. 2. Figure 3 displays the slowly varying RV motion of the A component, indicating that it is the ~0.2″ separation resolved component, whilst the B and C components display rapid RV motion, indicative of an unresolved tight spectroscopic binary. Figure 3 also indicates that the B+C pair are in anti-phase and have gone through ~180 degrees of motion, or some integer multiple of 180 degrees, between the 2010 and 2011 epochs (separated by ~90 days) and the 2014 and 2015 epochs (separated by ~80 days). Therefore, to first order we estimate the longest possible orbital period of the B+C pair to be ~170 days, and possibly factors of several shorter as multiple orbits may have been completed over the ~80 to 90 day baseline. Since the sampling of the RV data is very coarse relative to the period of the orbit, it is premature to attempt an exact orbital fitting. However, in order to acquire a tentative overview of which families of orbits would be feasible, we fit simple sine curves to the data, sampling the period from 1 to 170 days. In doing so, we consider the BC pair with the frame of reference fixed on component B, meaning we fit the sine curve to the $RV_C - RV_B$ data points. We find a best fit (minimum quadrature sum of the residuals) period of $P_{prel} = 3.4$ days, and a

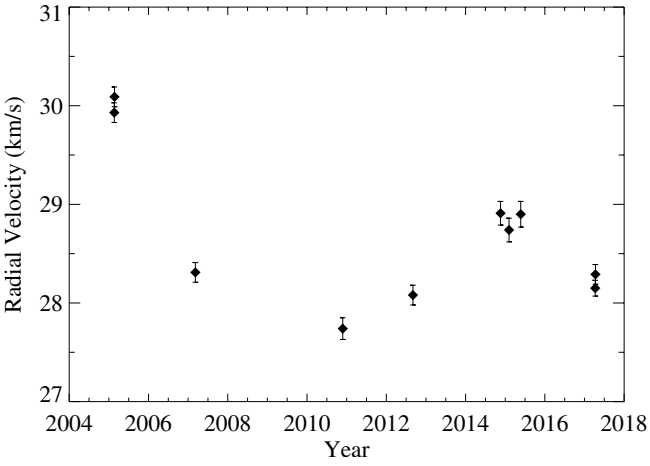

Fig. 1. Example RV plot featuring data measured for the single-lined J07285137−3014490 system. RV motion is evident and will be combined with astrometric data in order to constrain the system orbit; Rodet et al. (2018). The three data points between 2014 and 2016 were taken as part of this survey (programs 093.A−9006(A) and 094.A−9002(A)), the remainder come from archival and ongoing surveys.

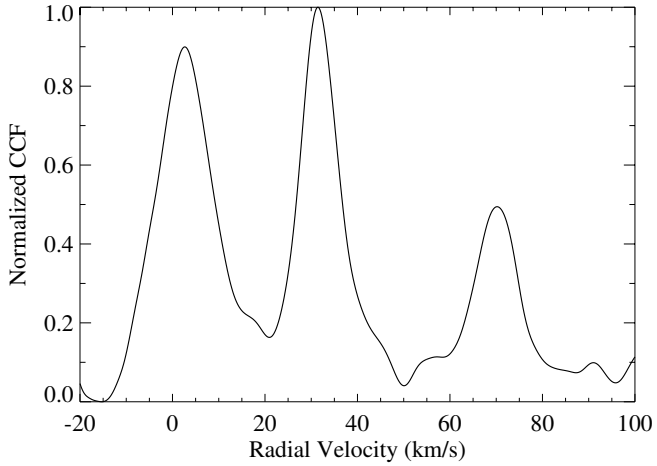

Fig. 2. Example CCF plot for the J053018 system. Three individual peaks are clearly distinguishable, and therefore we identify the system as a three-component spectroscopic multiple. Spectroscopic components are identified by tracing CCF peak strength across each epoch. We relate the strongest peak to the A component, occurring at ~30 km s^{-1}, the 2nd strongest peak to the B component, occurring at ~0 km s^{-1}, and the lowest strength peak to C component, occurring at ~70 km s^{-1}. The CCF displayed has been measured for MJD = 55525.295, across the 36th spectral order.

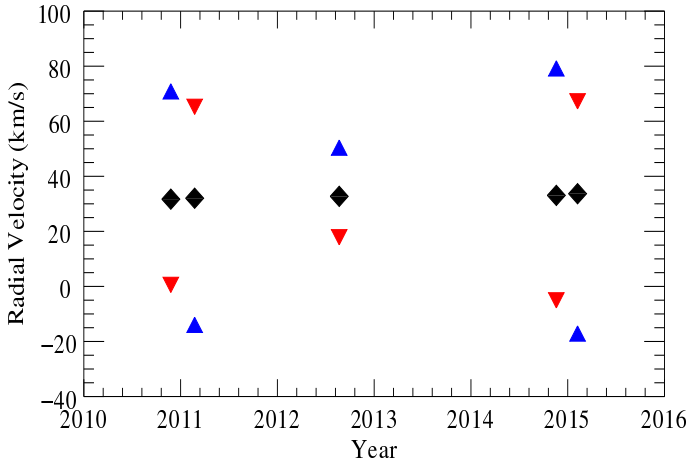

Fig. 3. RV data for the J053018 system. Errors are on the order of ~0.3 km s^{-1} and therefore lie within the data point boundaries. Color relates the measured RVs to indiviudal spectroscopic components; black = A component, red = B component, blue = C component, see text for details.

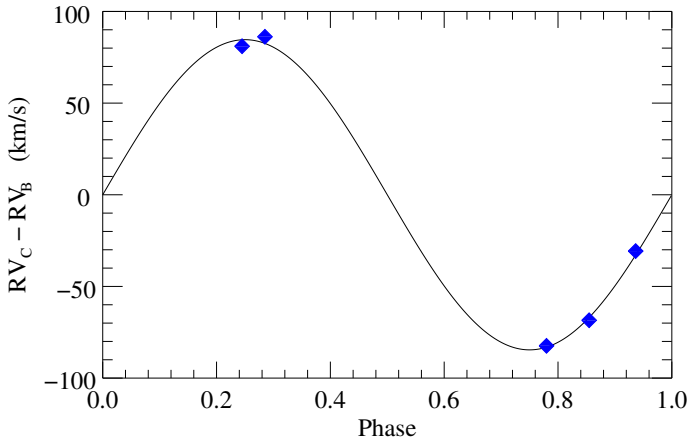

Fig. 4. Preliminary orbital fit to the J053018 BC system. BC component relative RVs (RV_C−RV_B) are plotted in blue as a function of orbital phase. Errors are on the order of ~0.4 km s^{-1} and therefore lie within the data point boundaries. Data is fit by a sine curve with a period of P_{prel} = 3.4 days, and a semi-amplitude of K_{prel} = 84.6 km s^{-1}.

semi-amplitude of $K_{prel} = 84.6$ km s^{-1}. The phase-folded fit is shown in Fig. 4. We reiterate that this is a preliminary fit and that future RV monitoring with a denser sampling will be needed for an unambiguous orbit determination. However, it is interesting to note that P_{prel} and K_{prel} are mutually consistent: If we assume a BC system mass of 0.3 $M_\odot$, based on individual spectral type (see following paragraph) and the relations of Kraus & Hillenbrand (2007), and a circular orbit, then the expected edge-on RV semi-amplitude for an orbital period of 3.4 days is 96.3 km s^{-1}. In projection, this is consistent with $K_{prel} = 84.6$ km s^{-1} if the inclination of the BC orbit is ~60 degrees. By contrast, if the orbital period were 10 days, then the expected edge-on RV semi-amplitude would be 65.5 km s^{-1}. This is too low to match the existing data points for a circular orbit. For longer periods, this discrepancy becomes increasingly pronounced. Hence a period in the <10 d range is favored by this argument.

Regardless of the specific orbit, as we can distinguish the B and C component RVs, we can measure the mass ratio and systemic RV of the pair following the methods of Wilson (1941). The component RVs are plotted against each other in Fig. 5 where the mass ratio of the pair is given by the negative of the gradient of the line. We measure a mass ratio of 0.75 ± 0.01 and a systemic RV of 31.2 ± 0.3 km s^{-1} for the pair. This systemic RV is consistent with the 31.3 ± 0.2 km s^{-1} RV measured for the M3.0 primary by Malo et al. (2014). This Malo et al. (2014) measurement is also consistent with the RV we measure for the slowly varying A component. We therefore identify the A component as the M3.0 primary and the M4.0 companion as the unresolved BC pair. We suspect the BC components are comprised of an M4.0+M5.0 pair. This is based on relating the mass ratio of the pair, and the relative strengths of the CCF peaks, to the unresolved M4.0 spectral subtype.

J053018 was previously thought to be a high probability member of the AB Dor YMG based on its kinematics with young age supported by significant X-ray emission (e.g., Lépine & Gaidos 2011; Janson et al. 2012). Using proper motions and their RV measurement for the M3 primary, Malo et al. (2014) derive an AB Dor membership probability of 97.7% using Bayesian Analysis for Nearby Young AssociatioNs (BANYAN, Malo et al. 2013), a statistical tool tracing YMG membership based on Galactic position and space velocity. As no trigonometric distance measurement exists for J053018, the BANYAN tool marginalizes this parameter in the YMG probability determination and generates the most probable statistical distance, 3 ± 1 pc, assuming membership to the AB Dor YMG is bona fide. We reevaluate the YMG membership using the BANYAN Σ tool (Gagné et al. 2018) and the systemic RV we measure for the BC pair. We find an AB Dor membership probability of >95% and a statistical distance of 2.5 ± 0.8 pc in agreement with the Malo et al. (2014) findings. However, whilst no trigonometric distance exists for J053018, Janson et al. (2012) derive a photometric distance of 23 ± 9 pc for the system. Unlike the statistical distance, this measurement is independent of any YMG membership assumption. At 23 ± 9 pc J053018 is highly unlikely to be an AB Dor member given its other kinematics and

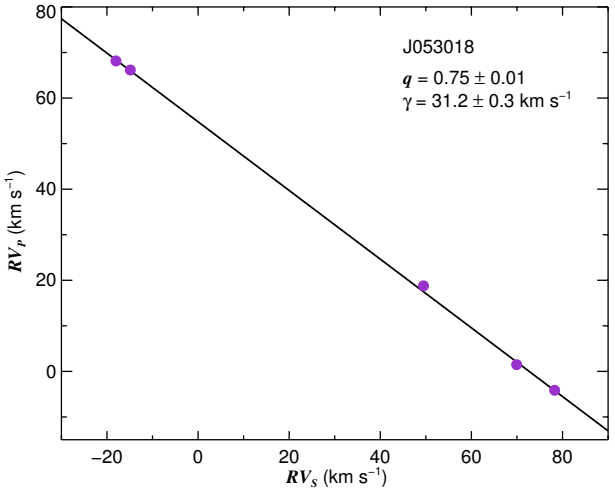

Fig. 5. J053018 B and C component RVs, denoted as RV_P and RV_S respectively. The negative gradient of the best-fit line is equal to the mass ratio of the system ($q = 0.75 \pm 0.01$), and we measure a systemic RV (γ) of 31.2 ± 0.3 km s^{-1}.

indeed, the BANYAN Σ tool returns a 0% membership probability. We suspect that this system is instead an old field interloper that appears young and X-ray active because the rotational velocities of the tight BC pair are high, due to spin-orbit locking. Enhanced chromospheric and coronal emission due to spin-orbit locking has previously been observed for the synchronized binary BF Lyn with an orbital period of ∼3.8 days (e.g., Montes et al. 2000; Maldonado et al. 2010). This argument is supported by a visual inspection of our FEROS spectra over Hα emission wavelengths. Figure 6 shows the Hα emission region of several epochs of spectra. In each epoch prominent emission lines are visible at the predicted Hα position given the measured RVs of the B and C components. However, no significant emission is visible at the predicted Hα position given the measured RV of the A component. This strongly suggests that the A component is no longer active because it is old, whilst the B and C components are active due to tidal spin-up. This argument is further reinforced by an inspection of the CCF peaks. As seen in Fig. 2, the B and C component peaks are significantly, ∼30%, broader than the A component peak. This is true across each epoch and usable order. Whilst this may be due to a mis-match with the cross correlation template, this suggests that the BC pair have larger rotational velocities than the A component, supporting the theory that the pair has been spun-up. The $P_{\rm prel} = 3.4$ day period is sufficiently short to allow the rotation of the components to be tidally locked to their orbit, and thus to be spun-up sufficiently to produce X-ray emission that matches the activity levels of a young (<100 Myr) population (e.g., Herbst et al. 2007).

4.2. The case of 2MASS J20163382−0711456

The system 2MASS J20163382−0711456, hereafter abbreviated as J201633, was previously known to be a M0.0+M2.0 resolved binary and a probable member of the Argus YMG. With a separation of ∼0.1″−0.2″, both components fall within the FEROS aperture. In each of our RV epochs we recover a single-peaked CCF and therefore identify J201633 as a single-lined binary. However, similar to the case of J053018, visual inspection of our FEROS spectra over Hα emission wavelengths suggests one of the components hosts an unresolved synchronized companion. Figure 7 shows the Hα emission region of a single epoch, which is representative of the series of observations. Again, no significant emission is visible at the predicted Hα position given the measured RV of the single lined system, however, emission lines are observed shifted to the blue and red of this position. We suspect the M0.0 primary is no longer active because the system is old whilst the M2.0 secondary is an unresolved synchronized pair which is active due to tidal spin-up, suggesting the system is an old field interloper. Due to the low signal to noise and similar heights of the resolved Hα peaks, we are unable to trace peak height across each epoch and relate specific Hα peaks to individual binary components.

Multiple studies (e.g., Malo et al. 2013, 2014; Janson et al. 2014b) have consistently identified J201633 as a probable Argus member using the BANYAN I and II tools, proper motions from the UCAC3 catalog (RA = 84.6 ± 8.1 mas yr^{-1}, Dec = -0.6 ± 23.6 mas $^{-1}$, Zacharias et al. 2009) and both marginalized (i.e., omitted) and photometric distances. We reevaluate the YMG membership using the BANYAN Σ tool and refined UCAC4 catalog proper motions (RA = 71.5 ± 3.9 mas yr^{-1}, Dec = 13.8 ± 3.5 mas yr^{-1}, Zacharias et al. 2012) and find a 99.9% probability that J201633 is a field star, given both marginalized and photometric (d = 50 ± 18.5 pc, Janson et al. 2014b) distance input parameters. However, the Argus group has been removed entirely from the models of BANYAN Σ, as it has been demonstrated to be composed of non-coeval stars (see Sect. 2). Given the BANYAN Σ field star probability and lack of Hα emission from the primary, it is highly likely J201633 is an old field interloper previously associated with the now doubtful Argus association. BANYAN Σ also returns a ∼99.9% field star probability for the remaining targets in the sample previously associated with Argus (see Table 2). However, each of these targets displays strong Hα emission due to the primary component and is highly unlikely to host a synchronizing companion around the primary (see Sect. 4.3). Therefore whilst these targets are young (<100 Myr), it is unclear if they are associated to any kinematic group. Unlike J053018, we do not detect any spectroscopic lines beyond Hα for the unresolved pair, and therefore cannot derive any individual RV measurements or generate an orbital fit. However, similar to J053018, we suspect the unresolved pair has a significantly short period, on the order of 1−10 days, in order for tidal synchronization to enhance X-ray emission that matches the activity levels of a young (<100 Myr) population (e.g., Herbst et al. 2007).

4.3. Limits on tidal synchronization

As the cases of J053018 and J201633 show, tidally synchronized pairs can mimick signatures of youth in low-mass systems, and can therefore critically bias isochronal analyses unless identified and discarded. Hence, we have scanned our sample for additional pairs of this nature, but only J053018, J201633 and the previously known J042442 system (with upper limit of 1.9 days on the orbital period of the BC pair, see Appendix A) show any such indications. In general, such systems should be easily identified, because at the necessary periods of <10 d for tidal synchronization to occur over ∼100 Myr timescales (see e.g., Meibom et al. 2006), they can be expected to have velocity semi-amplitudes of >30 km s^{-1}, similar to the J053018 system. However, there are two effects that can hide an otherwise detectable pair: (i) The system inclination may be very close to face-on, leading to a very small fraction of the total velocity to be projected into the measurable radial component.

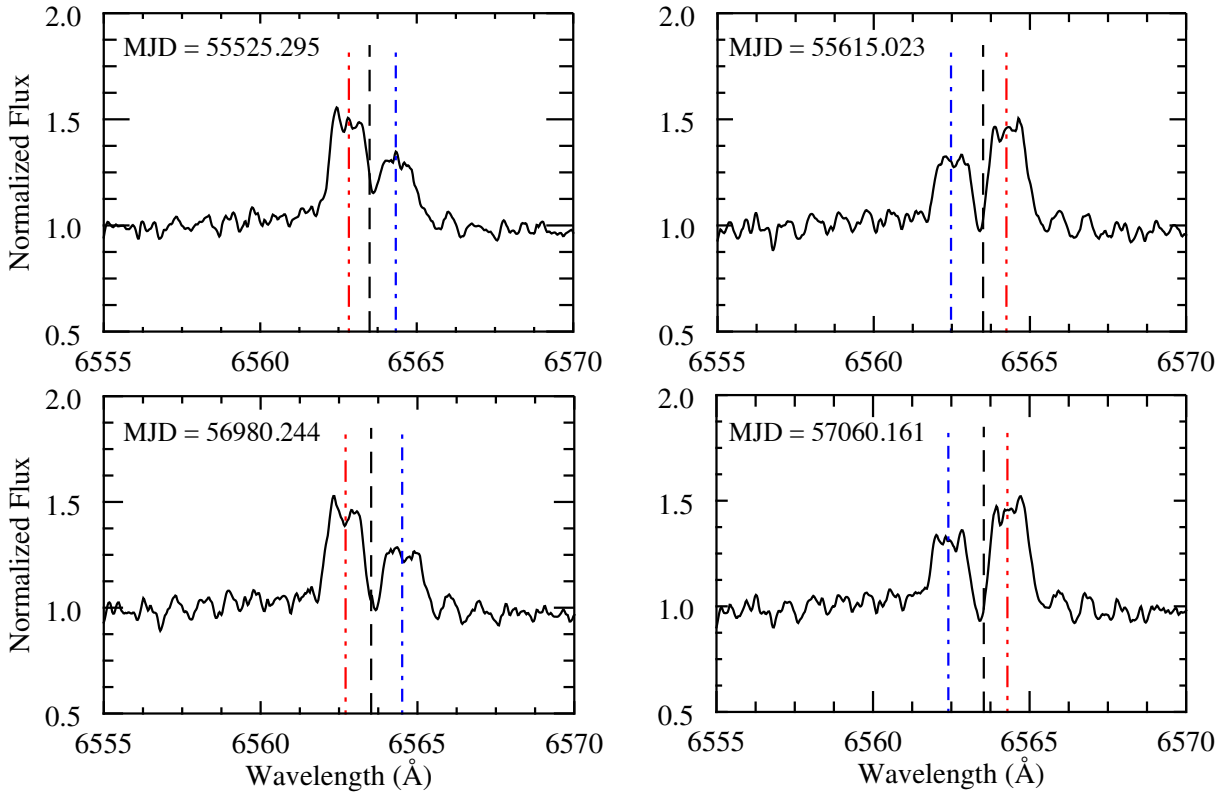

Fig. 6. Four epochs of J053018 FEROS spectra covering Hα emission wavelengths. The dashed lines highlight the predicted positions of the Hα emission line given the measured RVs of the A (black line), B (red line) and C (blue line) components. In each epoch, prominent emission lines are visible at the predicted Hα position given the measured RVs of the BC pair, whilst no emission is visible at the predicted Hα position given the measured RV of the A component.

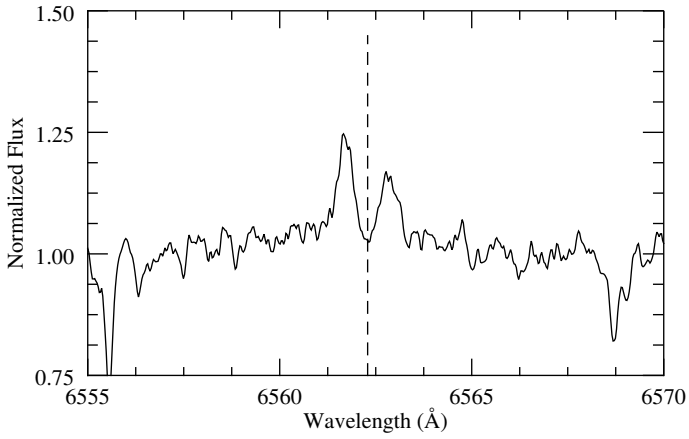

Fig. 7. J201633 FEROS spectra covering Hα emission wavelengths. The dashed line highlights the predicted position of the Hα emission line given the measured RV of the M0.0 primary. No emission is visible at this position. However, emission lines are observed shifted to the blue and red of this position. This suggests the M0.0 primary is no longer active because the system is old whilst the M2.0 secondary is an unresolved synchronized pair which is active due to tidal spin-up, resulting in Hα emission shifted according to the RV of the individual components.

(ii) Repeated RV measurements may accidentally sample the orbit in phases with similar instantaneous RV values. Both of these are low-probability effects, and the latter is particularly improbable if the RV has been sampled multiple times. Nonetheless, in a large enough sample, they should be expected to occur to some level, and it is therefore desirable to quantify to which extent they can be excluded for the targets in our sample without any detected signature. For this purpose, we have performed a series of Monte Carlo simulations for each individual target, as described in the following.

The total velocity semi-amplitude $K_{\rm tot}$ of a binary pair is a function of mass $M_{\rm s}$ of each individual known star that is hypothesized to host a synchronizing companion (hereafter named a "synchronizer"), the mass ratio q of the pair, and their eccentricity e and orbital period P. Whilst J042442 (see Appendix A), J053018 and J201633 host synchronizing companions around their secondaries, the remainder of the sample are identified as single-lined spectroscopic binaries that display Hα emission at the expected position given the measured RVs. Therefore if a synchronizing companion mimicking signatures of youth is present in these systems, it must orbit the primary component. Therefore, we only evaluate the presence of an unresolved synchronizer around this component in each system. Hence, $K_{\rm tot}$ is solely a function of the primary mass $M_{\rm s}$, q, e and P. Since we are interested only in tidally synchronized pairs in this analysis, the orbital periods will be limited to $P < 10$ d as mentioned above. Setting $P = 10$ d will thus provide a lower limit on $K_{\rm tot}$. In such short-period systems, eccentricities are known to be very low (e.g., Raghavan et al. 2010), which is a natural consequence of the same tidal forcing that causes the period synchronization. Hence, we set $e = 0$ in our simulations. The mass ratio distribution of close-in and low-mass systems is strongly peaked toward $q = 1$, and do not show $q < 0.5$ stellar systems even in surveys that are complete below this value (e.g., Reid & Gizis 1997;

Delfosse et al. 2004). Similarly to the P case, we thus set $q = 0.5$ to acquire a lower limit on $K_{\rm tot}$. The $M_{\rm s}$ masses are assigned individually for the targets in our sample, based on their spectral types following the same relation as in Janson et al. (2012).

For each system, we then perform 10^5 simulations in which $K_{\rm tot}$ is projected into a radial component assuming random orientations of the orbit. Since our observations are taken at irregular intervals that are generally much longer than 10 d, we can assume that such short orbits are effectively randomly sampled. We thus divide the velocity curve into a fine grid of small temporal segments, and randomly select $N_{\rm obs}$ segments for each of the 10^5 randomly projected orbits, where $N_{\rm obs}$ is the number of observations available for the target in question. We then evaluate the RV difference between adjacent pairs in the simulated ($\delta K_{\rm sim}$) and real ($\delta K_{\rm obs}$) observations, and choose the maximum among the $N_{\rm obs} - 1$ pairs in both cases. If $\max \delta K_{\rm sim} > \max \delta K_{\rm obs}$, it is considered that the hypothesized synchronizer should have been detected in this random instance, while the opposite is true if $\max \delta K_{\rm sim} < \max \delta K_{\rm obs}$. The fraction among the 10^5 simulations for a given target in which the synchronizer should have been detected is denoted $f_{\rm c}$. If $f_{\rm c}$ is close to 1, it means that there is virtually no way to hide a synchronizer, and so the hypothesis of its existence can be discarded. If $f_{\rm c}$ is small, there is not yet enough data to conclude whether a synchronizer might exist. The motivation for using adjacent pairs of observations as opposed to, for example, the minimum and maximum of the full set of observations is to mitigate the impact of the slower gradual RV trend that arises from the already known wider companions in the system.

All calculated $f_{\rm c}$ values are shown in Table 2. For the two systems J033235 and J052844, only one epoch of observations exists, and for the J042442, J053018 and J201633 systems a close companion has already been identified, so for those systems no meaningful $f_{\rm c}$ can be calculated. However, to test our methodology we compute $f_{\rm c}$ for the J053018 B component, as if we had not identified and measured RVs for the C component. Under these circumstances $f_{\rm c} = 0.0$, meaning there is no single case in which a simulated 10 day companion induces a larger RV variability than that measured for J053018 B. This is consistent, and therefore provides validation to our analysis, with a 10 day period corresponding to the minimal $K_{\rm tot}$ that could be caused by a synchronizer and the 3.4 day orbital period we estimate for the BC pair. For the other systems, $f_{\rm c}$ is generally very high – the lowest value is 0.799 for J061610, which still implies that it is unlikely that any synchronizer could hide from view, if such an object exists in the first place. The highest values are >0.999 for 5 systems, such that the synchronizer hypothesis can arguably be discarded entirely. This analysis implies that youth is the most probable explanation for high chromospheric activity in the vast majority of our sample, as is often supported also through kinematic YMG analysis. For J024514, there is point-to-point RV scatter significantly exceeding the formal errors, which could imply that a close-in companion exists. However, in this case the $f_{\rm c}$ of 0.964 implies that any such companion has a lower RV amplitude than would be expected from a synchronizer. In other words, while an additional unseen companion could exist in that system, it could not be responsible for the high activity level of the system. However, whilst the conclusion of youth remains probable in such a case, the presence of a non-synchronizing, unseen companion could lead to an incorrect isochronal age estimate or model calibration if the unresolved pair is treated as a single star. We estimate the frequency of such companions in our sample. The maximum separation limit of an unresolved companion is ~2.2 AU, given the approximate resolving power of AstraLux, 0.1″, and the typical target distance, ~22 pc. The minimum separation limit of a non-synchronizing companion is ~0.05 AU, given $P = 10$ days (as periods below this limit are required for tidal synchronization), a target mass of 0.245 $M_{\odot}$ (from Kraus & Hillenbrand 2007 for a typical survey target, SpT = M3.5) and q in the range 0.5–1.0. Fischer & Marcy (1992) give an indication of M-dwarf multiplicity over this approximate parameter space as they find 4 companions between 0.04 and 4.0 AU among 62 targets with a detection probability of 86%. Taken at face value this would give a multiplicity frequency of 7.5% in this range. Therefore, we adopt 7.5% as an upper frequency limit on 0.05–2.2 AU companions, as the derived (Fischer & Marcy 1992) frequency covers a broader separation range.

The value of $f_{\rm c}$ depends only weakly on the mass $M_{\rm s}$, but depends quite strongly on the number of data points acquired; with only two data points it is relatively easy to miss a high RV variability if (for example) two epochs are accidentally separated by an integer multiple of the periodicity, but with a larger number of irregularly spaced observations, this becomes exceedingly unlikely. However, high $f_{\rm c}$ values (>0.99) in the cases of J090758 and J205314 are derived as the RV variability has so little scatter that it is highly unlikely to catch a synchronizer with such minimal $\delta K_{\rm obs}$, even over just two randomly sampled data points.

5. Summary and conclusions

In this paper we have presented the results of an RV monitoring survey of a sample of 29 young M-dwarf multiples, many of which are high probability YMG members. These targets provide excellent laboratories for a range of astrophysical investigations and are prime candidates for isochronal analysis that can be used to calibrate low-mass stellar models and date individual systems. This dating can then potentially be applied to the full YMG of which they are members, for improved age constraints on the full population of stars. Our sample has been monitored through various astrometric monitoring campaigns, primarily our AstraLux multiplicity surveys, with the aim of deriving full orbital parameters and dynamical masses for the binary components. These model independent masses are essential for a robust isochronal analysis. Our RV measurements reported here complement the imaging data, allowing enhanced orbital determinations and precise dynamical masses to be derived in a shorter timeframe than possible with astrometric monitoring alone. Furthermore, as illustrated by the case of J053018, RV allows us to identify binary sub-pairs that are close enough to tidally synchronize, which increases their level of chromospheric activity. If such pairs go undetected, the age of the system can be drastically misestimated, which would invalidate any isochronal analysis. We have shown that the majority of our sample exhibits short-term RV variability on a level that is far lower than would be expected if they hosted $P < 10$ d stellar companions, even when accounting for the possiblity of unfortunate orbit projections or non-optimal orbit sampling. Thus, nearly all of our targets are best interpreted as genuinly young binaries with spatially resolvable orbits of a few years to decades, confirming their suitability for isochronal analyses. In future work, detailed orbital analysis and complementary spectral analysis of J043737 and J072851 (Rodet et al. 2018) will be presented.

Acknowledgements. S.D. acknowledges support from the Northern Ireland Department of Education and Learning. M.J. gratefully acknowledges funding from the Knut and Alice Wallenberg Foundation. C.A.W. acknowledges support by STFC grant ST/P000312/1. This work is based on observations made with

FEROS on the ESO-MPG 2.2 m telescope at La Silla Observatory. This study made use of the CDS services SIMBAD and VizieR, as well as the SAO/NASA ADS service.

References

Alonso-Floriano, F. J., Morales, J. C., Caballero, J. A., et al. 2015, A&A, 577, A128
Anglada-Escudé, G., Amado, P. J., Barnes, J., et al. 2016, Nature, 536, 437
Bailey, J. I., III, White, R. J., Blake, C. H., et al. 2012, ApJ, 749, 16
Baraffe, I., Chabrier, G., Allard, F., & Hauschildt, P. H. 1998, A&A, 337, 403
Baraffe, I., Chabrier, G., Barman, T. S., Allard, F., & Hauschildt, P. H. 2003, A&A, 402, 701
Baraffe, I., Homeier, D., Allard, F., & Chabrier, G. 2015, A&A, 577, A42
Barenfeld, S. A., Bubar, E. J., Mamajek, E. E., & Young, P. A. 2013, ApJ, 766, 6
Bate, M. R. 2012, MNRAS, 419, 3115
Bell, C. P. M., Mamajek, E. E., & Naylor, T. 2015, MNRAS, 454, 593
Bergfors, C., Brandner, W., Janson, M., et al. 2010, A&A, 520, A54
Bergfors, C., Brandner, W., Bonnefoy, M., et al. 2016, MNRAS, 456, 2576
Biller, B. A., Liu, M. C., Wahhaj, Z., et al. 2013, ApJ, 777, 160
Bonavita, M., Desidera, S., Thalmann, C., et al. 2016, A&A, 593, A38
Bonnefoy, M., Chauvin, G., Dumas, C., et al. 2009, A&A, 506, 799
Bonnet, H., Conzelmann, R., Delabre, B., et al. 2004, Proc. SPIE, 5490, 130
Brandeker, A., Jayawardhana, R., Khavari, P., Haisch, K. E., Jr., & Mardones, D. 2006, ApJ, 652, 1572
Brandt, T. D., Kuzuhara, M., McElwain, M. W., et al. 2014, ApJ, 786, 1
Burgasser, A. J., Reid, I. N., Siegler, N., et al. 2007, Protostars and Planets V, 427
Burrows, A., Sudarsky, D., & Lunine, J. I. 2003, ApJ, 596, 587
Calissendorff, P., Janson, M., Köhler, R., et al. 2017, A&A, 604, A82
Carpenter, J. M., Mamajek, E. E., Hillenbrand, L. A., & Meyer, M. R. 2006, ApJ, 651, L49
Chabrier, G., Johansen, A., Janson, M., & Rafikov, R. 2014, Protostars and Planets VI, 619
Chauvin, G., Lagrange, A.-M., Bonavita, M., et al. 2010, A&A, 509, A52
Close, L. M., Lenzen, R., Guirado, J. C., et al. 2005, Nature, 433, 286
Daemgen, S., Siegler, N., Reid, I. N., & Close, L. M. 2007, ApJ, 654, 558
Delfosse, X., Beuzit, J.-L., Marchal, L., et al. 2006, in Spectroscopically and Spatially Resolving the Components of the Close Binary Stars, eds. R. W. Hilditch, H. Hensberge, & K. Pavlovski (San Francisco, CA: ASP), ASP Conf. Ser., 318, 166
Delorme, P., Gagné, J., Girard, J. H., et al. 2013, A&A, 553, L5
Donati, J.-F., Catala, C., Landstreet, J. D., & Petit, P. 2006, Astron. Soc. Pac. Conf. Ser., 358, 362
Duchêne, G., & Kraus, A. 2013, ARA&A, 51, 269
Durkan, S., Janson, M., & Carson, J. C. 2016, ApJ, 824, 58
de Zeeuw, P. T., Hoogerwerf, R., de Bruijne, J. H. J., Brown, A. G. A., & Blaauw, A. 1999, AJ, 117, 354
Eisenhauer, F., Abuter, R., Bickert, K., et al. 2003, Proc. SPIE, 4841, 1548
Feigelson, E. D., Lawson, W. A., Stark, M., Townsley, L., & Garmire, G. P. 2006, AJ, 131, 1730
Fischer, D. A. & Marcy, G. W. 1992, ApJ, 396, 178
Fortney, J. J., Marley, M. S., Saumon, D., & Lodders, K. 2008, ApJ, 683, 1104
Gagné, J., Mamajek, E. E., Malo, L., et al. 2018, ApJ, 856, 23
Gillon, M., Triaud, A. H. M. J., Demory, B.-O., et al. 2017, Nature, 542, 456
Herbst, W., Eislöffel, J., Mundt, R., & Scholz, A. 2007, Protostars and Planets V, 297
Husser, T.-O., Wende-von Berg, S., Dreizler, S., et al. 2013, A&A, 553, A6
Janson, M., Brandner, W., Lenzen, R., et al. 2007, A&A, 462, 615
Janson, M., Bonavita, M., Klahr, H., et al. 2011, ApJ, 736, 89
Janson, M., Hormuth, F., Bergfors, C., et al. 2012, ApJ, 754, 44
Janson, M., Bergfors, C., Brandner, W., et al. 2014a, ApJ, 789, 102
Janson, M., Bergfors, C., Brandner, W., et al. 2014b, ApJS, 214, 17
Janson, M., Durkan, S., Hippler, S., et al. 2017, A&A, 599, A70
Kaufer, A., Stahl, O., Tubbesing, S., et al. 1999, The Messenger, 95, 8
Köhler, R. 2001, AJ, 122, 3325
Köhler, R., & Petr-Gotzens, M. G. 2002, AJ, 124, 2899
Köhler, R., Ratzka, T., Petr-Gotzens, M. G., & Correia, S. 2013, A&A, 558, A80
Konopacky, Q. M., Ghez, A. M., Duchêne, G., McCabe, C., & Macintosh, B. A. 2007, AJ, 133, 2008
Kraus, A. L., & Hillenbrand, L. A. 2007, AJ, 134, 2340
Kraus, A. L., Ireland, M. J., Martinache, F., & Lloyd, J. P. 2008, ApJ, 679, 762–782
Kraus, A. L., Shkolnik, E. L., Allers, K. N., & Liu, M. C. 2014, AJ, 147, 146
Lafrenière, D., Doyon, R., Marois, C., et al. 2007, ApJ, 670, 1367
Lafrenière, D., Jayawardhana, R., van Kerkwijk, M. H., Brandeker, A., & Janson, M. 2014, ApJ, 785, 47
Lawson, W. A., Crause, L. A., Mamajek, E. E., & Feigelson, E. D. 2001, MNRAS, 321, 57
Lépine, S., & Gaidos, E. 2011, AJ, 142, 138
López Martí, B., Jiménez-Esteban, F., Bayo, A., et al. 2013, A&A, 556, A144
López-Santiago, J., Montes, D., Crespo-Chacón, I., & Fernández-Figueroa, M. J. 2006, ApJ, 643, 1160
Luhman, K. L., & Steeghs, D. 2004, ApJ, 609, 917
Luhman, K. L., Joergens, V., Lada, C., et al. 2007, Protostars and Planets V, 443
Maldonado, J., Martínez-Arnáiz, R. M., Eiroa, C., Montes, D., & Montesinos, B. 2010, A&A, 521, A12
Malo, L., Doyon, R., Lafrenière, D., et al. 2013, ApJ, 762, 88
Malo, L., Artigau, É., Doyon, R., et al. 2014, ApJ, 788, 81
Mamajek, E. E., & Bell, C. P. M. 2014, MNRAS, 445, 2169
Meibom, S., Mathieu, R.D., & Stassun, K.G. 2006, ApJ, 653, 621
Montes, D., Fernández-Figueroa, M. J., De Castro, E., et al. 2000, A&AS, 146, 103
Montet, B. T., Bowler, B. P., Shkolnik, E. L., et al. 2015, ApJ, 813, L11
Müller, A., Roccatagliata, V., Henning, T., et al. 2013, A&A, 556, A3
Pecaut, M. J., Mamajek, E. E., & Bubar, E. J. 2012, ApJ, 746, 154
Quintana, E. V., Barclay, T., Raymond, S. N., et al. 2014, Science, 344, 277
Raghavan, D., McAlister, H. A., Henry, T. J., et al. 2010, ApJS, 190, 1
Rameau, J., Chauvin, G., Lagrange, A.-M., et al. 2013, A&A, 553, A60
Reid, I. N., & Gizis, J. E. 1997, AJ, 114, 1992
Reid, I. N., & Hawley, S. L. 2005, in New Light on Dark Stars Red Dwarfs, Low-Mass Stars, Brown Stars, eds. I. N. Reid, & S. L. Hawley (Praxis Publishing Ltd)
Riaz, B., Gizis, J. E., & Harvin, J. 2006, AJ, 132, 866
Rizzuto, A. C., Ireland, M. J., & Kraus, A. L. 2015, MNRAS, 448, 2737
Rodet, L., Bonnefoy, M., Durkan, S., et al. 2018, A&A, in press, DOI: 10.1051/0004-6361/201832924
Shkolnik, E. L., Hebb, L., Liu, M. C., Reid, I. N., & Collier Cameron, A. 2010, ApJ, 716, 1522
Song, I., Zuckerman, B., & Bessell, M. S. 2012, AJ, 144, 8
Stumpff, P. 1980, A&AS, 41, 1
Thalmann, C., Desidera, S., Bonavita, M., et al. 2014, A&A, 572, A91
Torres, C. A. O., Quast, G. R., Melo, C. H. F., & Sterzik, M. F. 2008, Handbook of Star Forming Regions, II, 5, 757
Tuomi, M., Kotiranta, S., & Kaasalainen, M. 2009, A&A, 494, 769
Vigan, A., Patience, J., Marois, C., et al. 2012, A&A, 544, A9
Vigan, A., Bonavita, M., Biller, B., et al. 2017, A&A, 603, A3
Vogt, S. S., Allen, S. L., Bigelow, B. C., et al. 1994, Proc. SPIE, 2198, 362
Walter, F. M., Vrba, F. J., Mathieu, R. D., Brown, A., & Myers, P. C. 1994, AJ, 107, 692
Wilson, O. C. 1941, ApJ, 93, 29
Zacharias, N., Finch, C., Girard, T., et al. 2009, VizieR Online Data Catalog: I/315
Zacharias, N., Finch, C. T., Girard, T. M., et al. 2012, VizieR Online Data Catalog: I/322
Zhou, G., Bayliss, D., Hartman, J. D., et al. 2014, MNRAS, 437, 2831
Zhou, G., Bayliss, D., Hartman, J. D., et al. 2015, MNRAS, 451, 2263
Zuckerman, B., & Song, I. 2004, ARA&A, 42, 685

Appendix A: Individual target discussion

J02490228−1029220. J024902 is a M1.5+M3.5+M3.5 resolved triple system for which we present three epochs of RV measurements. Bergfors et al. (2016) present an earlier FEROS spectrum of J024902, recording a RV of $17.1 \pm 1.1\,\mathrm{km\,s^{-1}}$ at MJD = 55901.121 along with a $v \sin i$ of $11 \pm 3\,\mathrm{km\,s^{-1}}$. Bergfors et al. (2016) also find J024902 to be a strong candidate member of the β Pic moving group, based on UVW galactic velocities and spectroscopic age indicators such as strong Li absorption. However, a parallax measurement is required to confirm group membership. Bergfors et al. (2016) additionally derive M4.0 ± 1.0 spectral types for both BC components from resolved SINFONI (Eisenhauer et al. 2003; Bonnet et al. 2004) spectra, consistent with the photometrically derived spectral types taken from Janson et al. (2012).

J04244260−0647313. J042442 is a previously known, three-component spectroscopic multiple, first reported in Shkolnik et al. (2010). We recover a triple-peaked CCF and derive RV measurements for all three components in each epoch of observations. An example triple-peaked CCF is shown in Fig. A.1. Figure A.2 shows the Hα emission region of a single epoch, which is representative of the series of observations. J042442 displays strong Hα emission at the predicted position given the measured RV of the primary. Shkolnik et al. (2010) estimate M4.5, M5.5 and M5.7 ± 0.5 component spectral types from HIRES (Vogt et al. 1994) and ESPaDOnS (Donati et al. 2006) spectra using the methods of Daemgen et al. (2007). Using the spectral type-mass relations of Reid & Hawley (2005) they then estimate component masses of 0.17, 0.12 and 0.1 $M_\odot$ and place an upper limit of 1.9 days on the orbital periods of the BC pair and 70.3 days on the orbit of the BC pair around the primary. As with J053018 and and J201633, we suspect that J042442 BC is a tidally synchronized pair as the 1.9 day orbital period is much shorter than the 10 day limit required for synchronization to occur over ∼100 Myr timescales (see e.g., Meibom et al. 2006). However, unlike J053018 and J201633, J042442 displays strong Hα emission at the predicted position given the measured RV of the primary. Therefore, J042442's X-ray emission is likely to be a genuine signature of youth, rather than due to tidal spin-up. Due to the tight nature of this system, <0.25 AU ($\lesssim$7 mas at 35 pc), it appears as a single star in our AstraLux images. Therefore, aside from possible interferometric applications, our derived RV measurements and planned future RV monitoring currently provide the only viable means to fully constrain orbital parameters and derive model independent component masses for this system.

J04373746−0229282 (GJ 3305). GJ 3305 is a bona fide β Pic moving group member (Malo et al. 2013) and has a rich amount of astrometric data points, spanning ∼15 yr of orbital motion. The binary is a wide (∼2000 AU, Feigelson et al. 2006) companion to the exoplanet host 51 Eri. It is a prime target for isochronal analysis that can be used to date the β Pic group and test mass-luminosity evolutionary models. This has been accomplished by Montet et al. (2015) who exploit the wealth of astrometric information and a sample of complementary RV data from the literature to derive full orbital parameters and component masses to a good level of precision. However, the mass uncertainties are dominated by the uncertainty in RV semimajor amplitude, resulting from a lack of sufficient RV data points. 7 epochs of RV measurements for GJ 3305 are presented here, increasing the sample of available RV data points by a factor of ∼2. Montet et al. (2015) find BHAC15 evolutionary models (Baraffe et al. 2015) to be consistent with individual component masses to within 1.5σ and derive a system age of 37 ± 9 Myr, consistent with the β Pic age of 24 ± 3 Myr (e.g., Bell et al. 2015; Mamajek & Bell 2014). This target is being densely monitored in both imaging and spectroscopy, and in future work, new orbital constraints will be deduced, with a considerable reduction in the error bars on the system age.

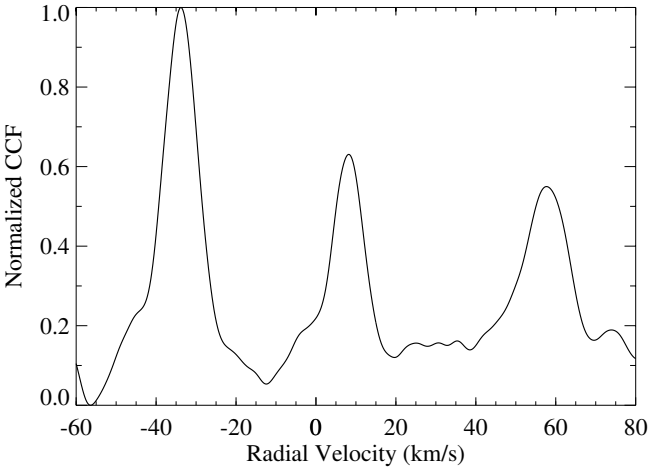

Fig. A.1. Example CCF plot for the J042442 system. Three individual peaks are clearly distinguishable, and therefore we identify the system as a three-component spectroscopic multiple. The CCF displayed has been measured for MJD = 55790.421, across the 35th spectral order.

J07285137−3014490 (GJ 2060). GJ 2060 is a bona fide AB Dor moving group member (Malo et al. 2013) and has a large spread of astrometric data, sufficiently sampling and closing the binary orbit. In this study we record 10 new RV measurements for GJ 2060 which are plotted in Fig. 1. These measurements will significantly aid in orbital determinations and place tighter constraints on individual component masses. A detailed orbital analysis of this system and complementary spectral analysis of the components is underway (Rodet et al. 2018).

J08475676−7854532 (EQ Cha). EQ Cha is a member of the η Cha association (López Martí et al. 2013) and a suspected unresolved binary. Its binarity was first suspected due to its elevation in the Hertzsprung-Russell diagram (Lawson et al. 2001; Luhman & Steeghs 2004). Surveys by Köhler & Petr-Gotzens (2002) and Brandeker et al. (2006) then revealed partially resolved images of J084756, supporting the binary nature of this system. By fitting the elongated, partially resolved PSF profile Brandeker et al. (2006) measure a binary separation of 40 mas (∼4 AU at 97 pc; Bonavita et al. 2016). This is within, or rapidly approaching, the diffraction limited resolution of the most advanced imaging instruments on 8 m class telescopes. Therefore, again aside from possible interferometric applications, our derived RV measurements and future RV monitoring currently provide the only viable means to produce a firm detection of the binary and derive orbital parameters and component masses.

J12072738−3247002 (TWA 23). TWA 23 is a bona fide member of the TW Hya association (Malo et al. 2014) for which we report three epochs of RV measurements in Table 2. We note that there exists two earlier epochs for this target listed in

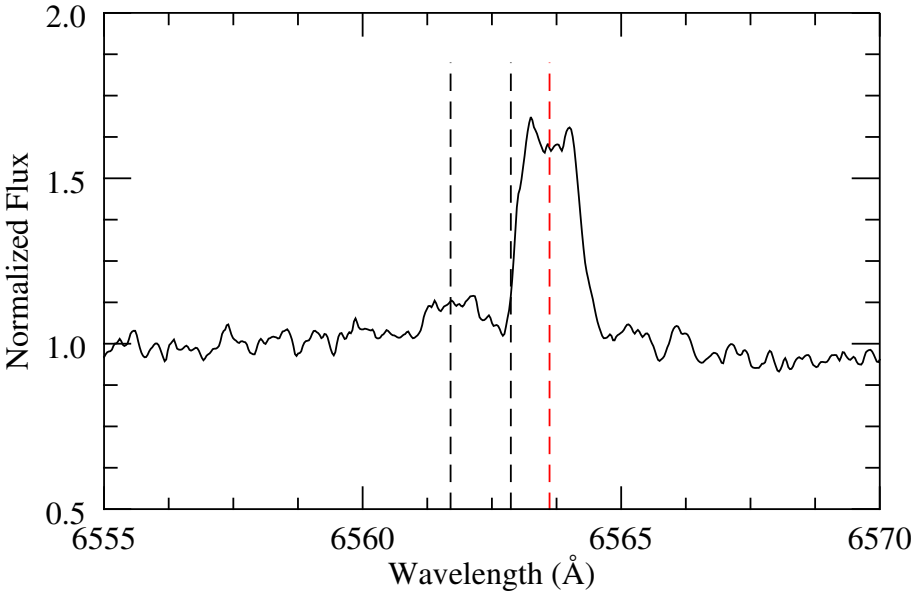

Fig. A.2. J042442 FEROS spectra covering Hα emission wavelengths. The dashed line highlights the predicted position of the Hα emission line given the measured RVs of the M5.5 and M5.7 BC pair (black lines–components indistinguishable) and the M4.5 primary (red line). Unlike J053018 and J201633, J042442 displays strong Hα emission at the predicted position given the measured RV of the primary. Hα emission is tentatively detected given the measured RV of one of the BC components and undetected given the other. This is a reasonable given the brightness contrast between the primary and the BC pair and the apparent RV separations.

the FEROS archive which we additionally reduce, identifying two distinct peaks in the CCF. This suggests the system is a two-component spectroscopic binary and that the individual CCF peaks have merged in our later epochs due to the binary motion and spectrograph resolution. However, we note that the coordinates listed in the archive for the earlier epochs are offset by ∼1.0′ from the actual target coordinates. Systems within a 2′ radius of TWA 23 are >6 magnitudes fainter, making it unlikely the target was misidentified within this region. However, Bailey et al. (2012) report RV measurements to a good level of precision (∼60 ms^{-1}) for this system, identifying it as a single-lined spectroscopic binary from well sampled observations over the same timescale as the estimated orbital period, ∼4 yr. This suggests the early archival FEROS epochs, displaying a double peaked CCF, are not reliable. As we can not confidently conclude whether or not TWA 23 was indeed observed during these epochs, we exclude the RVs measured for the components from Table 2, however we list them here for completeness; MJD = 54170.258, RV = −5.59 ± 0.22 and 19.10 ± 0.41 km s^{-1}; MJD = 54228.241, RV = −3.51 ± 0.25 and 17.66 ± 0.41 km s^{-1}.

J15573430−2321123. J155734 is a high probability member of the Upper Scorpius subgroup of the Sco-Cen association (Rizzuto et al. 2015). Kraus et al. (2008) resolved this system using aperture masking interferometry, deriving a binary separation of ∼50 mas and estimating a mass ratio of 0.59 ± 0.06 from the measured contrast following the methods of Kraus & Hillenbrand (2007). Lafrenière et al. (2014) partially resolve the system and use a template to fit the elongated PSF profile to measure binary separation and contrast, which they use to estimate a mass ratio of 0.39 with uncertainties on the order of 10−30%. This system will notably benefit from our measurements and future RV analysis over a longer baseline, allowing the mass ratio discrepancy reported in the literature to be resolved and full orbital parameters to be derived for this tight binary.

J20531465−0221218. J205314 is a potential member of the Argus moving group (Malo et al. 2013) for which we report two epochs of RV measurements in Table 2. As with TWA 23, we note there exists an additional archival epoch, which we reduce to recover a double peaked CCF, suggesting the system is a two-component spectroscopic where the individual CCF components have merged during our later epochs. Again however, the coordinates listed are offset by ∼1.0′ from the actual target coordinates. As we can not confidently conclude whether or not J205314 was observed in this archival epoch, we treat this system in a similar fashion to TWA 23 and exclude the data from Table 2, but list our measurements here for completeness; MJD = 56809.274, RV = −45.32 ± 0.24 and −32.50 ± 0.30 km s^{-1}.

J23205766−0147373. J232057 is a high probability member of the Argus moving group (Malo et al. 2014) and was resolved by Daemgen et al. (2007) with a separation of ∼0.1″. However, the system has since appeared as a single star in our AstraLux images, indicating that the binary companion has moved inward. Our RV measurements are of significant importance for this system as they provide the most viable means of sampling the orbital motion over this timeframe, until the two components become visible again.